# Measurement of Surface Hydrophobicity of Engineered Nanoparticles using Atomic Force Microscope

| | |
|---|---|
| Journal: | *Physical Chemistry Chemical Physics* |
| Manuscript ID | CP-ART-07-2018-004676.R1 |
| Article Type: | Paper |
| Date Submitted by the Author: | 27-Aug-2018 |
| Complete List of Authors: | FU, WANYI; New Jersey Institute of Technology, Civil and Environmental Engineering<br>Zhang, Wen; New Jersey Institute of Technology, Department of Civil and Environmental Engineering; New Jersey Institute of Technology, |
| | |

# Measurement of Surface Hydrophobicity of Engineered Nanoparticles using Atomic Force Microscope

Wanyi Fu and Wen Zhang*

John A. Reif, Jr. Department of Civil and Environmental Engineering, New Jersey Institute of Technology, Newark, New Jersey 07102, United States

*Corresponding author: 323 Martin Luther King Blvd., Newark, NJ 07102; Phone: (973) 596-5520; Fax: (973) 596-5790; Email: wen.zhang@njit.edu

## Abstract

Determination of surface hydrophobicity or wettability of nanomaterials and nanoparticles (NPs) is often challenged by heterogeneous properties of NPs that vary with particle size, shape, surface charge, aggregation states, and surface sorption or coating. This study first summarized inherent limitations of water contact angle, octanol-water partition coefficient ($K_{ow}$) and surface adsorption of probe molecules in probing nanomaterial hydrophobicity. Then, we demonstrated the principle of a scanning probe method based on atomic force microscopy (AFM) for the local surface hydrophobicity measurement. Specifically, we measured the adhesion forces between functionalized AFM tips and self-assembly monolayers (SAMs) to establish a linear relationship between adhesion force and water contact angles based on the continuum thermodynamic approach (CTA). This relationship was used to determine local surface hydrophobicity of seven different NPs (*i.e.*, $TiO_2$, ZnO, $SiO_2$, CuO, $CeO_2$, α-$Fe_2O_3$, and Ag), which agreed well with bulk contact angles of these NPs. Some discrepancies were observed for $Fe_2O_3$, $CeO_2$ and $SiO_2$ NPs, probably because of surface hydration and roughness effects. Moreover, the solution pH and ionic strength had negligible effects on the adhesion forces between the AFM tip and MWCNT or $C_{60}$, indicating that hydrophobicity of carbonaceous nanomaterials is not influenced by pH or ionic strength (IS). By contrast, natural organic matters (NOM) appreciably decreased the hydrophobicity of MWCNT and $C_{60}$ due to surface coating of hydrophilic NOM. This scanning probe method has proved to be reliable and robust toward the accurate measurement of nanoscale hydrophobicity of individual NPs or nanomaterials in liquid environments.

## 1. Introduction

Extensive use of anthropogenic nanomaterials in industries and consumer products has increased the likelihood of their exposure to the natural environment. Consequently, the concern over the potential toxicity of nanoparticles (NPs) to the environment and human health is indisputably mounting. Extensive research has demonstrated that metal oxide NPs (*e.g.*, $TiO_2$, ZnO, and $Fe_2O_3$) can disrupt cell membrane surfaces,[1-3] induce cytotoxicity[4, 5], cell penetration,[6] and uptake by gastrointestinal cell lines.[1, 7, 8] Effective characterization of physicochemical properties of engineered nanoparticles (ENPs) is critical to understanding their potential fate, transport, and bioavailability.[9, 10] Accurate measurement of interfacial properties of ENPs is also important for the development of functional nanomaterials for diverse environmental or industrial applications.

### 1.1. Impact of hydrophobicity on fate and transport of NPs in aqueous environment

Among numerous nanomaterial properties (*e.g.*, size, shape, surface charge, and coating), surface hydrophobicity or hydrophilicity (also known as wettability) has pivotal impacts on their stability, fate, transport, and interfacial interactions such as inter-particle repulsion or attraction. For example, water molecules adhere to hydrophilic NPs and form steric layers on their surfaces, which may prevent other particles or molecules to approach or interact with. Alternatively, if the relative affinity of water molecules toward particle surface is lower than that between NPs themselves, rapid attraction and aggregation of NPs will occur, which is termed as hydrophobic attraction or hydrophobic effect.[11] Therefore, surface hydrophobicity affects particle stability and interfacial processes (*e.g.*, molecular adsorption).

Hydrophobic NPs may preferentially partition to hydrophobic regions of cell membrane and result in a higher potential of accumulation and penetration across the cells.[12, 13] For example, hydrophobic nanomaterials like carbon nanotubes or graphene have a tendency to partition into the lipid bilayer of cell membrane, which strongly affect the biological toxicity of NPs.[14, 15] Therefore, developing suitable characterization methods for probing surface hydrophobicity at nanoscale is indispensable for comprehensive understandings of environmental processes and cell interactions of NPs.

**1.2. Factors affecting surface hydrophobicity**

Nanomaterial hydrophobicity is difficult to assess due to dynamic changes and processes (*e.g.*, protein sorption and corona formation) of nanomaterials upon their release into the environment. For example, transition-metal oxides, such as $TiO_2$ and ZnO, are well-known to exhibit photo-induced hydrophilicity under UV irradiation.[16, 17] Hematite ($\alpha$-$Fe_2O_3$) surface also demonstrated switchable hydrophobicity from superhydrophobicity to superhydrophilicity and vice versa with $UV_{254}$ irradiation and dark storage.[18] Moreover, hydrophobicity shift could also be ascribed to the adsorption of proteins (*e.g.*, albumin and fibronectin) and natural organic matters (NOM) in natural environment, which may greatly alter their surface properties. For example, $C_{60}$ that is hydrophobic can be shifted to hydrophilic by surface hydroxylation by means of oxidation and thus hydroxylated $C_{60}$ are more easily dispersed in water compared to pristine $C_{60}$, thereby resulting in different environmental fate and transport. Additionally, adsorption of hydrophobic organics may induce appreciable hydrophobic interactions and particle aggregation.

Besides, the design and synthesis of ENPs for various applications often require specific surface coatings or functionalization, which render special surface chemistries and hydrophobicity.[19, 20] For instance, hydrophobic NPs such as polymeric NPs are used for bioremediation of hydrophobic contaminants.[21] Chitosan or chitosan-DNA NPs serve as new vehicles in drug and gene deliveries.[22] Likewise, functionalized gold NPs (fGNPs) can be modified to hydrophobic in drug delivery applications to increase the delivery efficiency.[23]

Clearly, determination of surface hydrophobicity of NPs is challenged by aqueous environment factors and heterogeneous properties of NPs that potentially depend on morphology (size and shape), surface charge, aggregation states, and surface sorption or coating. For example, surface energy of nanomaterials could be dependent on size and shape,[24, 25] surface structures,[26] and lattice parameters.[27] During the last few decades, intensive efforts have been made to develop experimental methods to accurately determine local surface hydrophobicity of NPs. Reported methods that are used to probe nanomaterial hydrophobicity include the measurements of water contact angle, octanol-water partition coefficient ($K_{ow}$) and surface adsorption of probe molecules.[28]

### 1.3. Current characterization methods for nanomaterial hydrophobicity and their limitations

***(1) Contact angle measurements***

Contact angle measurement (CAM) has long been used as a criterion of static hydrophobicity of solid surfaces. It is a simple-to-adopt method for surface hydrophobicity analysis based on the sessile drop Young–Laplace method. Surfaces with small water contact angles (<30°) are usually called hydrophilic surfaces, while for

contact angles higher than 90°, the surface is considered as hydrophobic. Water contact angle reflects an average hydrophobicity of macroscale flat solid surfaces. Kuna *et al*.[26] found that the local hydrophobicity may be influenced by the nanoscale features of the materials and thus the bulk water contact angles may not directly indicate local surface hydrophobicity of individual NPs at the liquid interface.

Contact angles (CA) exhibit dependence on the position of liquid drops on heterogeneous material surfaces.[29, 30] For example, the contact angle measurement could be influenced by surface roughness, surface contamination or coating and the gas pocket trapped in the interparticle void space on the film (lotus effect).[31, 32] One example is that a perfectly pure gold surface is hydrophilic but due to carbon contamination in crystal lattice most gold surfaces appear slightly hydrophobic.[33] Because NPs tend to interact with NOM (*e.g.*, humic acid and fulvic acid), proteins and salts in the environment,[34, 35] the typical surface groups on NPs may include $–NH_2$, –OH and –COOH as well as common cations and anions (*e.g.*, $Na^+$, $Ca^{2+}$, $Cl^-$ and $SO_4^{2-}$). Thus, most metallic and metal oxide NPs in the environment should be close to hydrophilic.

Although microscopy has been utilized to measure localized water contact angles on sample surface,[36] high-resolution of nanoscale visualization of liquid drops is still not achieved. To tackle this problem, a gel trapping technique (GTT) was developed to determine contact angles of individual colloidal particles at liquid surfaces.[37, 38] As illustrated previoulsy,[37] NPs were trapped at the surface of an aqueous gel, molded with curable poly(dimethylsiloxane) (PDMS), which was lifted up and imaged with high-resolution camera to determine the contact angles at the air−water or oil−water interface. In addition, SEM, X-ray microscopy, confocal microscopy and atomic force microscopy

122 (AFM) have been applied to assist the visualization of local contact angles.[37, 39, 40] In
123 practice, contact angle is difficult to measure accurately for colloidal particles, because
124 the particle surface and the interface are optically unclear. Besides, the GTT method
125 requires complicated sample preparations, which introduces uncertainties or artifacts.

126 ***(2) Partition coefficient ($K_{ow}$) measurement***

127 Some studies proposed employing the octanol-water partitioning coefficient ($K_{ow}$) to
128 represent surface hydrophobicity of NPs.[41-43] $K_{ow}$ is typically defined as the mass ratio of
129 a molecular concentration in octanol phase to its concentration in water. This ratio
130 reflects the partitioning affinity of the tested molecules to the organic phase. A high $K_{ow}$
131 generally indicates that the chemical molecules have high tendency to partition into
132 organic phases and may pose greater potential to enter and accumulate in biological
133 interfaces. For example, DDT (di(pflra-chlorophenyl)-trichloroethane) or dioxins are
134 hydrophobic pollutants that have high $K_{ow}$ values. However, the theoretical basis of $K_{ow}$ is
135 established on molecular partitioning processes that the tested substances can diffuse
136 between water/organic phases, which is not applicable for insoluble NPs or
137 nanomaterials.[28, 44] Also, the NPs render different processes, such as transport,
138 aggregation and accumulation at phase interfaces, which make it impossible to achieve
139 the thermodynamic conditions for an equilibrium distribution of nanomaterials. Thus,
140 partitioning experiments can hardly reflect the real hydrophobicity properties of
141 individual NPs and may lead to erroneous predictions of environmental fate.[44] Finally,
142 partitioning coefficients renders no information on nanoscale material hydrophobicity.

143 ***(3) Hydrophobic or hydrophilic probe molecules method***

144 Surface adsorption of different hydrophobic or hydrophilic probe molecules (*e.g.*, p-
145 xylene, chlorobenzene, naphthalene and phenol) was reported to evaluate the relative
146 hydrophobicity/hydrophilicity of nanomaterials.[28, 45-47] Briefly, the quantities of the probe
147 molecules absorbed on nanomaterial surfaces and in the media are measured at
148 equilibrium to obtain the adsorption coefficients. The plot of adsorption coefficients
149 against the total particle surface area yields a straight line, where the slope of the line was
150 taken as the measure of surface hydrophobicity/hydrophilicity. If the probe compounds
151 are hydrophobic, the larger the slope, the more hydrophobic nanomaterials are. If the
152 probe molecules are hydrophilic, the larger the slope, the less hydrophobic the particle
153 is.[28, 47] This method has been used to measure the surface hydrophobicity of
154 microparticles that enable the targeted intracellular delivery of therapeutics.[48] Although
155 this method is demonstrated well on nanomaterials of all sizes, it potentially yield
156 misleading information due to the inherent heterogeneous and dynamic characteristics of
157 NPs in aqueous phase. For instance, adsorption kinetics and equilibrium are highly
158 sensitive to and dependent on available surface areas of NPs, which may be prone to
159 aggregation and have reduced surface area for adsorption. Moreover, aggregation kinetics
160 could become more complicated and unpredictable in the presence of the added
161 hydrophobic or hydrophilic probe molecules. Moreover, the adsorption modes (Langmuir
162 or Freundlich) of probe molecules on NBs are difficult to determine. Fang *et al*. measured
163 the surface energy of NPs by monitoring the adsorption capacity for water molecules
164 from the surrounding vapor, which is similar to the Brunauer, Emmett, and Teller (BET)
165 technique for surface area measurements.[49] However, the adsorption saturation on NPs is

166 hard to differentiate because of the potential multiple layered deposition of water or other
167 molecules on the surface of NPs.

168 **1.4. Applications of scanning-probe methods with AFM**

169 AFM has proven useful in the assessment of a suite of surface properties including
170 hydrophobicity at both microscale and nanoscale, such as soil particles,[50] microbial
171 cells,[51] polymeric membranes,[52] and nanostructured surface/thin film.[31, 53, 54] These
172 previous studies showed that the interfacial force measurement on AFM is shown to
173 reveal surface energies[55] and hydrophilic or hydrophobic characteristics of the interacting
174 surfaces.[54] AFM utilizes a sharp tip (e.g., 10–15 nm of radius of curvature) to measure
175 the adhesion force that arises from adhesive bonds between the two interacting surfaces.[25]
176 Based on the continuum thermodynamic approach (CTA), adhesion energy is related to
177 the macroscopic observations of contact angles (*e.g.*, the Young-Dupré equation) and
178 potentially renders hydrophobicity of the probed sites.[26, 51] Noel *et al.* also found that the
179 adhesion force measured between AFM tips and self-assembled monolayers (SAMs) of
180 different functional groups (*e.g.*, methyl, ester and amine), increased linearly with the
181 surface energy determined with contact angles.[56] For nanomaterials, it remains elusive if
182 such correlation or agreement exists between adhesion energy and water contact angle.
183 Clearly, a direct correlation will allow us to better probe nanoscale surface
184 hydrophobicity and crystallographic orientation or facet-dependent surface energy of
185 nanocrystals.[57, 58]

186 **1.5. Relationship of adhesion work and hydrophobicity**

187 To engage the AFM probe tip to contact a sample surface, external work is applied to
188 expel solvent or water molecules that adsorb on both tip and samples surfaces. Once in

contact, the functional groups of probe tips and sample surfaces will establish hydrogen bonding or other adhesive bonding. To break up the contact, the tip will be pulled to overcome the adhesion force ($F_{ad}$) as shown in **Figure 1a** and adhesion energy ($W_{ad}$). $W_{ad}$ can be obtained from the integration in the force-distance curve ($W_{ad} = \int F_{ad} \mathrm{d}Z$, where $Z$ is the interaction distance) as shown in the triangle gray area in **Figure 1a**. $W_{ad}$ is related to the model of Johnson, Kendall, and Roberts (JKR model) by:

$$\frac{W_{ad}}{\pi \cdot a^2} = \frac{F_{ad}}{1.5\pi \cdot R_c} = \gamma_L - \gamma_L \cdot \cos\theta_{SL} \quad (1)$$

where $W$ is the adhesion energy per unit contact area in the JKR equation, $F_{ad}$ is the adhesion force, $R_C$ is the radius of curvature for the cantilever tip (nm) that is determined by SEM, and $a$ is the contact site radius. Thus, the adhesion energy is equal to the increase of surface energy in the red box in **Figure 1b** after the tip is pulled up:[59]

$$W_{ad} = (\gamma_{SL} + \gamma_{TL} - \gamma_{TS}) \cdot \pi \cdot a^2 \quad (2)$$

where $\gamma_{SL}$, $\gamma_{TL}$ and $\gamma_{TS}$ are the interfacial energies between the sample surface and liquid interfaces, between the tip surface and liquid interfaces, and between the tip and sample surface, respectively (mJ m$^{-2}$). Eq. (2) is supported by the depletion attraction mechanism in the Asakura–Oosawa theory,[60] which indicates that when the two surfaces contact, water molecules are stripped from the interspace and water molecules outside the two surfaces will exert pressure on the two contact bodies, which enhances the attraction between the two surfaces as shown in **Figure 1b**. The free energy is released when the surfaces of two surfaces come into contact because of the changes and reconstruction of surface energy (solvation layers).[60] According to the Dupré equation, $\gamma_{SL}$, $\gamma_{TL}$ and $\gamma_{TS}$ can be further expressed as:

$$\gamma_{SL} = \gamma_S + \gamma_L - W_{SL} \quad (3)$$

$$\gamma_{TL} = \gamma_T + \gamma_L - W_{TL} \quad (4)$$

$$\gamma_{TS} = \gamma_T + \gamma_S - W_{TS} \quad (5)$$

Eqs. (3)-(4) indicate that the interfacial energies are directly linked to solid (sample and tip) and liquid solvent surface energies ($\gamma_S$, $\gamma_T$ and $\gamma_L$) and the work of adhesion ($W_{SL}$, $W_{TL}$ and $W_{TS}$).[26] $W_{SL}$ can be deduced from the water contact angle using the Young equation:

$$W_{SL} = \gamma_{LV}(1+\cos\theta_{SL}) \approx \gamma_L(1+\cos\theta_{SL}) \quad (6)$$

where $\gamma_{LV}$ is the interfacial energy between the liquid and vapor interface (mJ m$^{-2}$), $\theta_{SL}$ and $\theta_{TL}$ are the contact angles between the probe liquid and sample and tip surfaces. $W_{TL}$ is equal to $W_{TS}$ if the tip only involves London dispersion interactions with the solvent molecules or sample surfaces.[51] Combining Eq. (2)-(6) yields the relationship between $W_{ad}$ and contact angles:

$$W_{ad} = (\gamma_S - \gamma_L \cdot \cos\theta_{SL} + \gamma_T - \gamma_L \cdot \cos\theta_{TL}) \cdot \pi \cdot a^2 \quad (7)$$

Eq. (7) can be converted to adhesion force-based form according to the JKR model:

$$W = \frac{W_{ad}}{\pi a^2} = \frac{F_{ad}}{1.5\pi R_c} \quad (8)$$

Eq. (8) indicates that adhesion force ($F_{ad}$) is linearly related to the contact angle ($\theta_{SL}$) and the surface tension of probe liquids ($\gamma_L$). Thus, by measuring the adhesion force, we can quantitatively and precisely measure the local contact angle ($\theta_{SL}$) at the resolution of the contact site area ($\pi \cdot a^2$). In contrary, the traditional contact angle measurement of $\theta_{SL}$ is a measure of macroscopic surface hydrophobicity of the bulk materials. Besides, the

relation in Eq. (7) or (8) is a more generalized form than that proposed by Alsteens *et al.*,[51] who only derived the relation for $CH_3$-modified tip and $CH_3$-/OH-modified sample surfaces. Eq. (7) or (8) is applicable for different tip-sample interactions and enables us to probe the surface hydrophobicity at nanoscale. The following sections will experimentally verify the applicability of Eq. (7) or (8) by testing different self-assembled monolayers (SAMs) surfaces with known contact angles and further on seven different NPs.

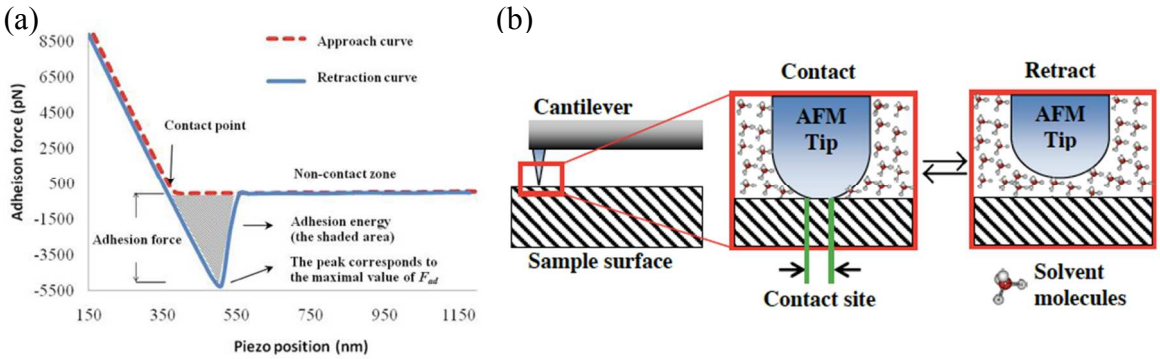


**Figure 1**. (a) Representive force-distance curve from which adhesion force ($F_{ad}$) and adhesion energy ($W_{ad}$) were calculated. (b) Scheme of adhesion force measurement with AFM and the Asakura–Oosawa theory employed to calculate the free energy changes between the contact and retraction states of AFM tip against sample surface.

To overcome the sizable limitations of the conventional measurement of surface hydrophobicity for nanomaterials, this study demonstrated a scanning-probe method with atomic force microscopy (AFM) to accurately determine local surface hydrophobicity through the measurement of adhesion force between functionalized AFM probe tips and sample surface. The adhesion force was then converted to contact angle values ("nanoscale water contact angles"). In our study, four types of hydrophilic or hydrophobic self-assembly monolayers (SAMs), namely, polyethylene glycol (PEG), biotin, streptavidin, and silane, were used to create ultra-smooth and well-ordered

252 structures surfaces that warranted homogeneous tip-sample interactions. Different NPs
253 including $CeO_2$, hematite ($\alpha$-$Fe_2O_3$), $TiO_2$, ZnO, CuO, $SiO_2$, Ag, $C_{60}$, and multiwall
254 carbon nanotube (MWCNT) were prepared and immobilized on a silicon substrate and
255 then probed by chemically functionalized AFM tips. Adhesion forces were also assessed
256 under different solution pH, ionic strength (IS), and the presence of NOM.

257 **2. Experimental**

258 **2.1. NPs and characterization**

259 All NPs were purchased from commercial sources as summarized in **Table S1** in the
260 supporting information. Water suspensions of different NPs (*i.e.*, $TiO_2$, ZnO, $SiO_2$, CuO,
261 $CeO_2$, $\alpha$-$Fe_2O_3$, and Ag with citric acid coating) were made by dispersing the powers into
262 deionized (DI) water (Millipore, 18.2 MΩ). The NP suspension was sonicated (Misonix
263 sonicator S-4000, Qsonica, LLC). NPs were immobilized on clean and flat silicon
264 undoped (N-type) wafer surfaces with surface orientation (100) via spin-coating on a spin
265 coater device (Laurell WS-400E). The silicon wafer was cleaved into small pieces of
266 about 3 mm × 8 mm. Immerse them in 2% ultrapure nitric acid solution for 30 min and
267 then use 90% high purity ethanol to rinse it rigorously. Finally, DI water was sprayed
268 onto the silicon surface to remove any residual impurities on the surface and place the
269 clean silicon chips in a Petri dish. A typical thin layer of NPs was achieved by dropping
270 200 μL of the NP suspension with a mass concentration of approximately 100 mg $L^{-1}$ on
271 the substrate and spun at 3000 rpm for 5 min. Finally, samples were air dried for 5-10
272 min before measuring water contact angles. Morphology and sizes of NPs were
273 determined by transmission electron microscopy (TEM, Philips EM420) at 47-120 kV.

Hydrodynamic diameters of NPs were determined by a dynamic light scattering (DLS) instrument (Nano ZS Zetasizer, Malvern Instruments).

To ensure the tip-sample interactions in AFM force measurement, a full surface coverage of deposited NPs on substrate surface must be achieved. However, the depth of the deposited NPs (in multilayer or monolayer) is not controlled and does not likely affect the adhesion force measurements, because the adhesion force is measured on the outer surface of the deposited NP layers (the inner or deeper surface of layered NPs are not accessible by AFM probes).

**2.2. Preparation of SAM substrate surface**

To establish the linear correlation between adhesion force and water contact angle, we measured the adhesion forces between AFM tips and alkanethiol SAMs terminated with -OH and -$CH_3$ groups in DI water.[51] Briefly, gold-coated silicon (100) wafers were immersed in ethanol solutions containing 1 mM $HS(CH_2)_{11}CH_3$ (CAS No. 112-55-0, Sigma-Aldrich) and $HS(CH_2)_{11}OH$ (CAS No. 73768-94-2, Sigma-Aldrich) in various proportions (e.g., 0:100-100:0) for 14 h and then rinsed with ethanol before use. In addition, four other SAMs including poly(ethyleneglycol) (PEG), hydrophobic silane, biotin, and biotin-streptavidin conjugates (MicroSurfaces Inc. USA) were coated on 2×2 cm glass slides to verify the correlation. Water contact angles were measured on these functionalized substrate surfaces with a Model 250 Ramé-hart goniometer at ambient conditions.

**2.3. Functionalization of AFM probe tips**

Two kinds of AFM cantilevers were used in the experiments to compare the coating effects on adhesion force measurements. One was gold-coated silicon nitride ($Si_3N_4$)

297 cantilevers (RC800PB, Asylum Research, USA), and the other was non-coated $Si_3N_4$
298 cantilevers (MCLT, Veeco, USA). Before the functionalization, the tips were rinsed with
299 deionized water and then methanol to remove any surface contaminants from probes.
300 Hydrophobic cantilevers were obtained by functionalizing the gold-coated $Si_3N_4$
301 cantilevers with $-CH_3$ groups following the same method as described in our previous
302 work.[52] The detailed information of all the cantilevers are summarized in **Table S2**.

303 **2.4. Adhesion force measurement with AFM**

304 First, adhesion force between the modified tip and the surfaces of mixed self-
305 assembled monolayers (SAM) of $CH_3$- and OH-terminated alkanethiols was measured in
306 DI water according to the method of Alsteens *et al*.[51] The hydrophobicity of the SAM
307 surfaces was varied due to the different molar fractions of $CH_3$-alkanethiols present on
308 the gold surface (100 % $CH_3$-terminated alkanethiols is the most hydrophobic while 100%
309 OH-terminated alkanethiols is the most hydrophilic). The measured adhesion forces were
310 plotted versus the corresponding molar fraction of $CH_3$-alkanethiols.

311 The immobilized NPs on silicon wafer were rinsed with DI water to remove any
312 loosely bonded NPs and then placed in a liquid cell containing DI water or other
313 desirable solutions for at least 15 min before the adhesion force measurement. Samples
314 images were first acquired by AFM at scanning speeds varying from 2000-5000 nm $s^{-1}$,
315 depending on the image quality. The AFM probe tips were engaged onto the NPs
316 surfaces at least 50-70 different locations to collect the force-distance curves and generate
317 a histogram of adhesion force distribution for each sample (**Figure S2** and **S3**). Detailed
318 operation of AFM in force mode and the quality check procedure are provided in **Section**
319 **S2** and **S3** in the SI.

320 **2.5. The effects of ionic strength, pH and NOM on the hydrophobicity of MWCNT**
321 **and $C_{60}$**

322 The pH of the MWCNT or $C_{60}$ solutions was adjusted to 3.5, 7.0, and 9.0 by 0.1 M
323 NaOH or 0.1 M HCl while the ionic strength of the suspension after the adjustment was
324 less than 10 mM to minimize the ionic strength effect on surface states or charges of NPs.
325 When studying the effect of ionic strength, the solution pH was maintained at pH 6.0 ±
326 0.2 while the ionic strength was varied from 0.01, 0.025, 0.05, 0.075, to 0.1 M by adding
327 KCl. MWCNT or $C_{60}$ were immobilized on silicon wafer by air drying a drop of the
328 suspension, which were then placed in above liquid cell containing the solution of
329 different pH or ionic strength for 15 min to reach steady state or equilibrium of ion
330 adsorption on NPs. Finally, the force measurement was conducted on AFM following the
331 same procedure as described in **Section 2.4**.

332 To study the NOM effect, humic acid (HA, Sigma) was prepared in DI water (600 mg
333 $L^{-1}$) with overnight stirring in the dark. The solution was then filtered under vacuum
334 using a 0.22-μm membrane filter (Whatman), adjusted to pH 6.0 ± 0.2, and subsequently
335 stored in the dark at 4 $^{o}$C. To achieve sufficient surface coating or adsorption of humic
336 acid on MWCNT or $C_{60}$, 100 μL of the NP suspension was mixed with 200 μL of the
337 humic acid stock solution, followed by vortexing (Mini Vortexer, Fisher Scientific) to
338 homogenize the suspension.[61] The mixture suspension was left in the dark for 2 h to
339 permit adsorption equilibrium, followed by centrifugation at 10,000×*g* for 5 min to settle
340 the NPs from water. After the supernatant was discarded, NPs was responded by DI water
341 and rinsed twice to remove loosely bound humic acid on the surface of NPs. The humic
342 acid-adsorbed NPs were then deposited on the silicon wafer for the AFM analysis.

### 2.6 Statistical analysis

The measured contact angles were obtained with at least triplicate sampling and testing. The calculated contact angles with adhesion forces were obtained with 50-70 force curves. The presented results are mean values ± standard deviation. The differences between calculated and measured contact angles, and the differences between test groups were tested for significance using t-test at a significant level of 0.05.

## 3. Results and Discussions

### 3.1. Water contact angles on surfaces of NPs

**Table S3** and **Table S4** summarized the water contact angles for different NPs, gold surface coated with different amounts of -$CH_3$ groups and different SAM surfaces. The surface hydrophobicity follows an order of $TiO_2$ > $Fe_2O_3$ > CuO > $CeO_2$ > $SiO_2$ > ZnO > AgNPs coated with citrate acid. When the advancing water contact angle ($\theta$) on the surface is less than 15$^o$, the hydration force becomes significant and stabilizes the colloidal suspension, which explains the stable dispersion of $TiO_2$ or $Fe_2O_3$ NPs. By contrast, hydrophobic forces become appreciable when $\theta$ >64$^o$ and particle aggregation or coagulation may take place.[62]

### 3.2. Adhesion force measurement between functionalized tips with different surface functionalization and SAMs

Our results in **Figure 2a** indicated that adhesion forces for different tips all increased as the molar fraction of $CH_3$-alkanethils increased, which is consistent with previous literature.[26, 51] Compared to the gold tip coated with $CH_3$ ligands, the bare gold tips and $Si_3N_4$ tips also yielded similar dependence but a lower level of adhesion force. Moreover,

the plots of adhesion forces and the values of $-\cos(\theta_{SL})$ showed good linearity in **Figure 3b-d**, which matches our model relation in Eq. (8). The linear fitting for $CH_3$-gold tip led to a correlation coefficient of 0.98, higher than those of bare gold tips or $Si_3N_4$ tips.

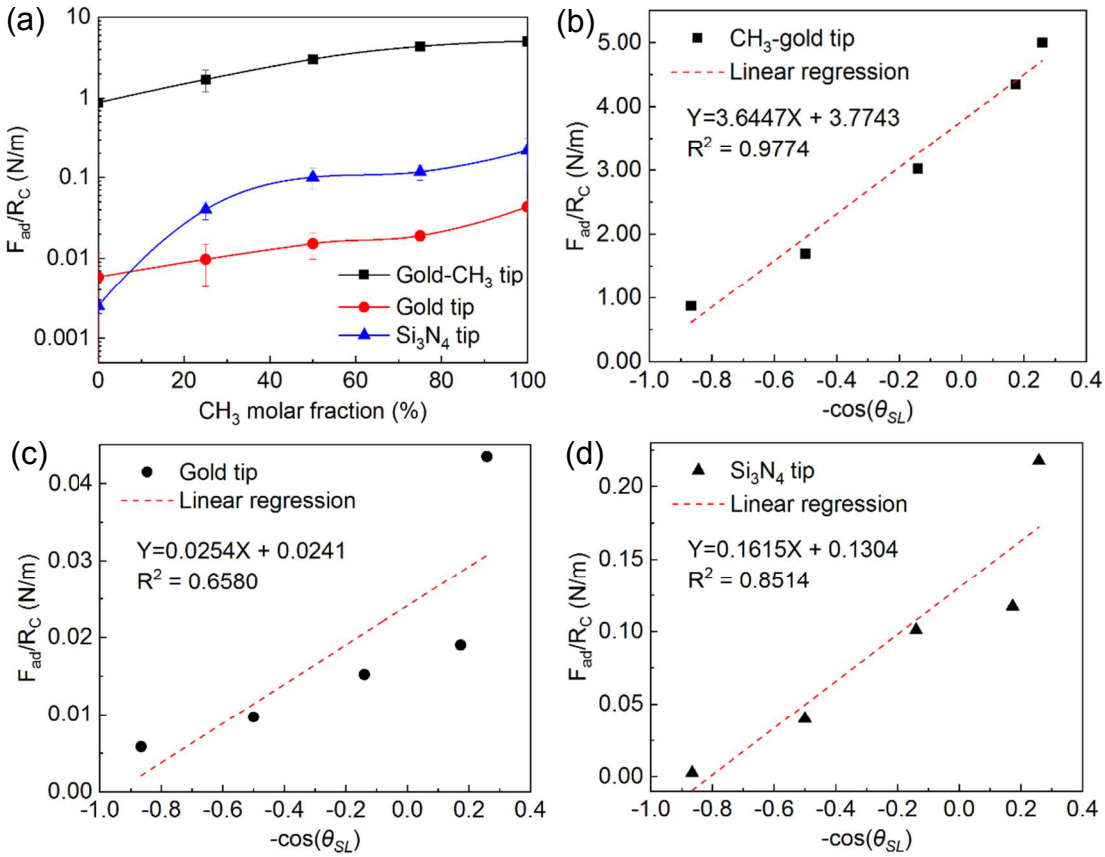


**Figure 2.** (a) Adhesion force as a function of the surface fraction of $CH_3$-terminated alkanethiols. (b)-(d) are the linear curve fitting for the results of $F_{ad}/R_c$ and $-\cos(\theta_{SL})$ for gold tips w/o $-CH_3$ coating and uncoated $Si_3N_4$ tip.

The adhesion forces between the three types of AFM tips and four different SAM surfaces are shown in **Figure 3a**. **Figure 3b-c** shows the linear curve fitting for adhesion forces versus the values of $-\cos(\theta_{SL})$. The two uncoated AFM tips, however, yielded poorer linearity as indicated by the fluctuations of adhesion forces on the hydrophilic SAM surfaces (*e.g.*, PEG, biotin, and streptavidin). Previous work indicated that the correlation between adhesion force and surface energy is highest for the $-CH_3/-CH_3$

378 molecules on the interacting surfaces,[63] compared to other interacting molecular groups
379 (–COOH/–COOH, –$CH_3$/–COOH, –$CH_3$ or –COOH/octenyl-trichlorosilane). This
380 supports our results that -$CH_3$ coated gold tips yielded strong linear dependence on
381 adhesion force and negative cosine of water contact angles.

382 According to Eq. (8), the linear equation should have a slope equal to the surface
383 energy of water ($\gamma_L$), which is 72.8 mJ $m^{-2}$ or 0.0728 N $m^{-1}$ at 25 $^{o}$C. This is close to the
384 slope (0.10 N $m^{-1}$) fitted from the data for SAM surfaces in **Figure 3b**. However, the
385 experimentally fitted slope may vary slightly due to surface interaction characteristics.[64,
386 65] For example, in addition to hydrophobic interactions, other non-specific binding and
387 molecular anchoring may also contribute to surface adhesion, which explains the
388 discrepancies of the fitted slope values from the surface energy of water ($\gamma_L$).

389

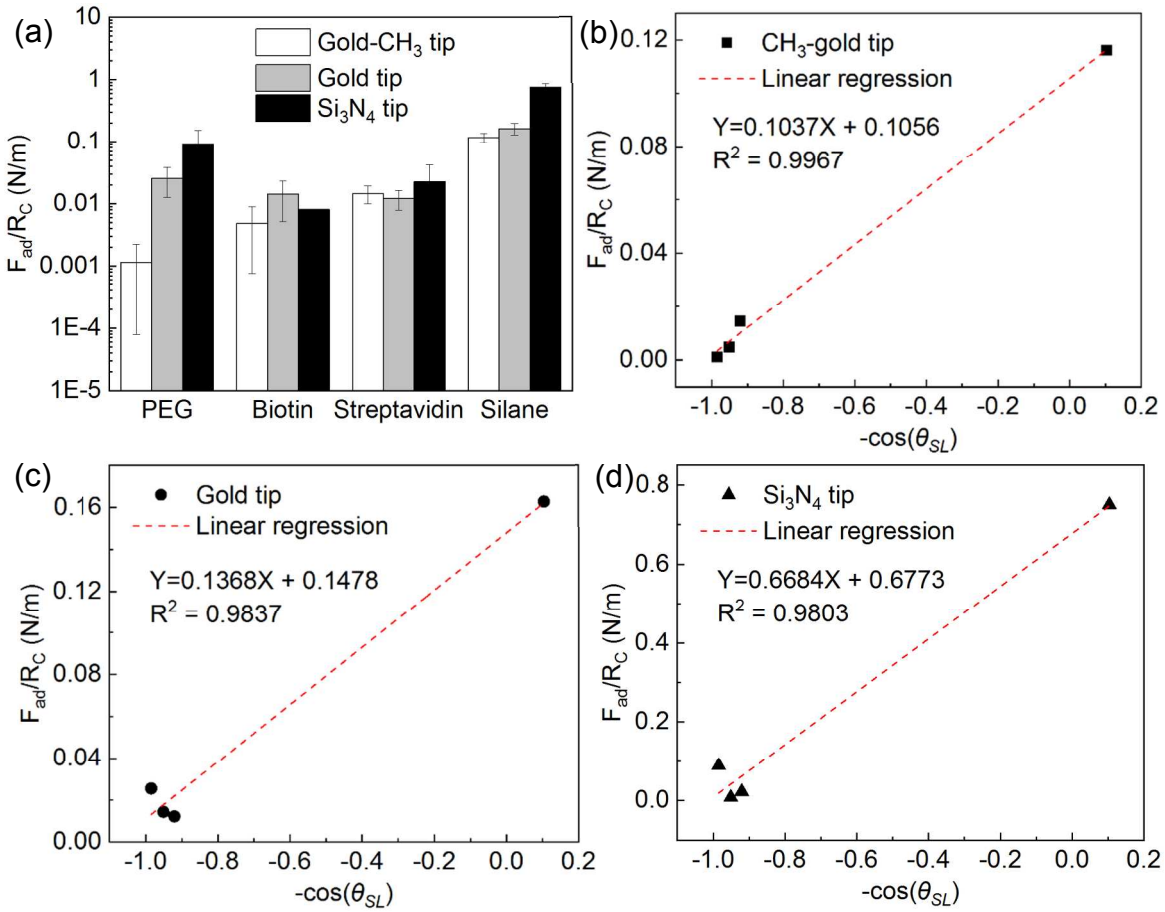


**Figure 3**. (a) Adhesion forces between three types of tips and different SAM surfaces. (b)-(d) Adhesion forces versus the value of -cos($\theta_{SL}$) for three types of tips.

### 3.3. Adhesion force measurement between the $CH_3$-coated gold tip and different NPs

To calculate water contact angles from adhesion forces, we employed the linear equation in **Figure 3b** as the "calibration equation". **Figure 4** shows that the contact angles calculated from adhesion forces were almost equal to the experimental measurements of bulk water contact angles for $TiO_2$, ZnO and CuO NPs. However, some subtle discrepancies ($p$ <0.05) existed for $Fe_2O_3$, $CeO_2$, $SiO_2$, and AgNPs, probably due to the effect of hydration on interfacial energy at nanoscale.[26, 66] According to Chiu *et al.*,[66] a local hydration effect can be caused by the curvature of the particle-water

interface such that the surface hydrophobicity may shift from hydrophobic for ultra-small NPs to hydrophilic properties for large particles. Our previous study examined the nanoscale hydrophobicity of chemically modified polyethersulfone membranes and also found this subtle discrepancy between the bulk water contact angle and experimentally derived from adhesion forces, which was attributed to the surface roughness effect or the lotus leave effect.[52]

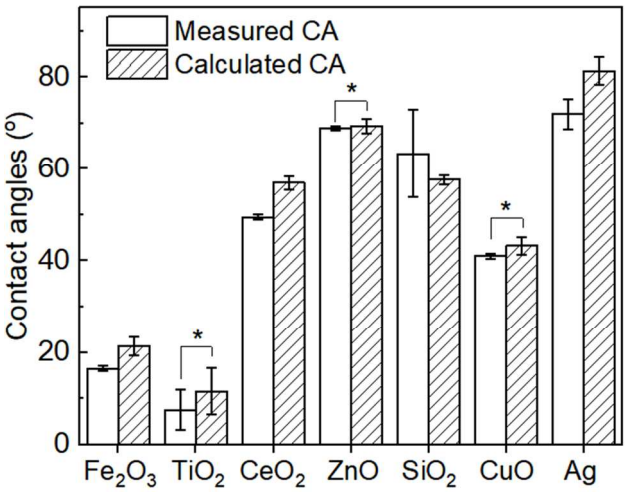


**Figure 4.** Comparison between calculated and experimental contact angles for seven kinds of NPs. * indicates no significant difference ($p > 0.05$).

### 3.4. Effects of water chemistries and surface coating on hydrophobicity of MWCNT and $C_{60}$

MWCNT and $C_{60}$ were used as model hydrophobic nanomaterials to evaluate the effects of the solution pH, IS, and NOM on the adhesion force measurement or the surface hydrophobicity of nanomaterials. **Figure 5** shows that MWCNT was characterized to be super-hydrophobic (the bulk water contact angles, *ca.* 150 $^{o}$) and $C_{60}$ was hydrophobic (the bulk water contact angle, *ca.* 120 $^{o}$), which was consistent with the

419 previous studies.[67, 68] Our results indicate that pH had little influence on the measured and
420 calculated CAs from adhesion forces on MWCNT (**Figure 5a, b**). The average measured
421 CAs for MWCNT were ~146 $^{o}$ over the pH range (3.5-9.0), while the calculated CAs
422 decreased slightly from ~170 $^{o}$ to ~130 $^{o}$. Similarly, no significant differences were found
423 between the measured CAs for $C_{60}$ under different pHs. Meanwhile, the calculated CAs
424 for $C_{60}$ increased from 72 $^{o}$ to 90 $^{o}$ when pH increased from 3.5 to 9.0. Different from
425 MWCNT, significant differences ($p$ <0.05) between calculated and measured CAs were
426 observed for $C_{60}$ over the pH range (3.5–9.0), suggesting the deposition of $C_{60}$ on silica
427 surface was not homogenous at bulk scale and nanoscale. It is reported that the deposition
428 of the $C_{60}$ NPs on silica surface was mostly irreversible and $C_{60}$ NPs may detach at high
429 solution pHs.[69] Thus, the bulk CA measurement may likely include silicon wafer surfaces
430 without $C_{60}$, especially when the pH was high (pH = 9.0). Nevertheless, this AFM probe
431 method directly probes the surface of NPs and thus can apparently avoid potential
432 artifacts from the sample displacement.

433 **Figure 5c** shows no significant differences between the calculated and measured CAs,
434 regardless of the ionic strength variations, indicating that there was a negligible effect of
435 ionic strength on hydrophobicity of MWCNT. Though a decrease in the measured CAs
436 and an increase of the calculated CAs of $C_{60}$ were observed when the ionic strength
437 increased from 10 mM to 25 mM, there was no clear dependence for contact angles on
438 ionic strength. The negligible effects of pH and IS on the hydrophobicity of MWCNT
439 and $C_{60}$ probably because hydrophobic MWCNT and $C_{60}$ had low surface interactions
440 such as sorption of charged ions on MWCNT or $C_{60}$.[70] Though many previous studies
441 reported the effects of pH and ionic strengths on the aggregation behaviors of MWCNT

or $C_{60}$ NPs, there was no report about hydrophobicity impacts from the changing pH or IS. It is reported that the surface tension and the contact angle of hydrophobic ethyl cellulose NPs at the interface all remain unchanged under different ionic strengths,[71] which supports our observation that hydrophobic interactions among NPs are insensitive to the solution IS.

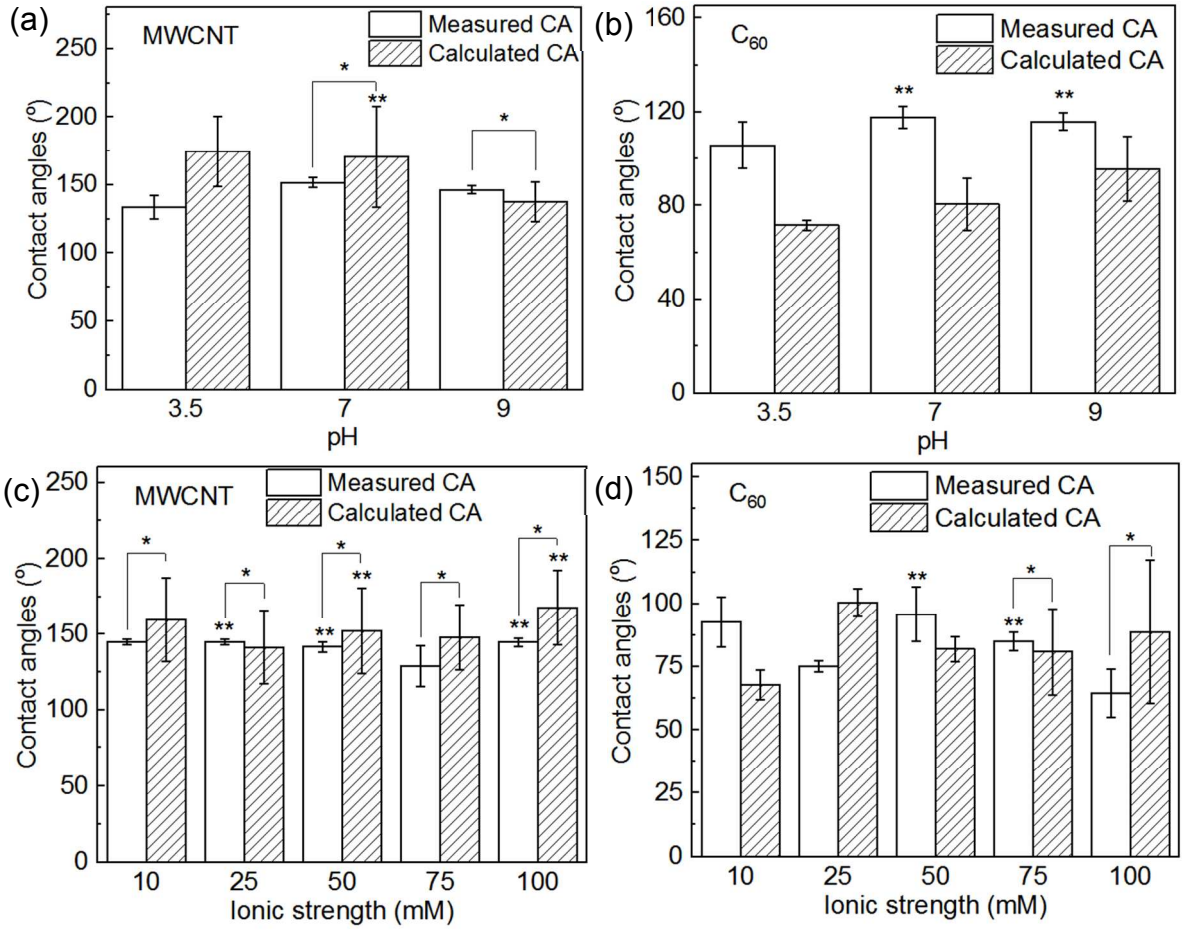


**Figure 5**. Effects of pH (a, b) and ionic strength (c, d) on the contact angles measurements of $C_{60}$ and MWCNT. * indicates no significant difference ($p$ >0.05) between measured and calculated contact angles. ** indicates no significance in comparison to control groups ($p$ >0.05). Control group: pH = 3.5 or IS = 10 mM.

**Figure 6** shows that the coating of HA substantially decreased the hydrophobicity of MWCNT and $C_{60}$ as indicated by the decline of water contact angles, which has

commonly been reported in literature.[72-74] Due to the hydrophobic effect induced by the aliphatic components of HA, they could adsorb on carbonaceous materials (*e.g.*, MWCNT) via π–π interaction, hydrogen bonding or Lewis acid–base interactions,[75-77] which ensured a stable and repeatable AFM analysis. After adsorption of HA, MWCNT and $C_{60}$ presented hydrophilic surfaces due to the hydrophilic domains in HA molecular. By contrast, the coating or surface deposition of HA on metal or metal oxide NPs may change due to dissolution and result in potential discrepancies of adhesion force measurements. Nevertheless, with the surface coating by HA, we believe the hydrophobicity shift for metal/metal oxide NPs should be similar with the results on MWCNT and $C_{60}$ as the adhesion force is primarily contributed by tip-HA interactions.

On the other hand, obvious discrepancies between calculated and measured CAs were observed for HA coated carbon-based nanomaterials and the measured CA was smaller than the calculated ones. This could be attributed to the uneven adsorption of HA on nanomaterials, making some of the local surfaces of MWCNT or $C_{60}$ remain uncoated or partially coated, which thus exhibited higher level of hydrophobicity. This also implies that AFM-based method for hydrophobicity probing may reveal higher resolution and greater accuracy for nanomaterial characteristics.

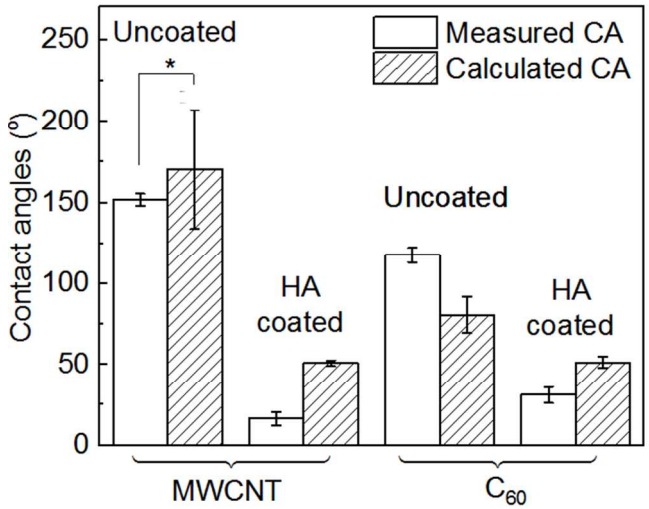


**Figure 6**. Effects of HA coating on the contact angles measurements of $C_{60}$ and MWCNT. * indicates no significant difference ($p$ >0.05) between measured and calculated contact angles.

## 4. Conclusions

Accurate characterization of nanomaterial hydrophobicity is critical for modeling and predicting the fate and transport of NPs, including aggregation, adsorption, deposition, and biological interactions. Undoubtedly, this presented scanning probe method provides an unparalleled and stable approach to evaluate authentic hydrophobicity of nanomaterials at nanoscale, which are different from the conventional methods. The findings unravel new insights that localized surface heterogeneity (e.g., roughness, surface hydration and coating) of nanomaterials could make their nanoscale surface hydrophobicity differ from macroscopic surface hydrophobicity as commonly indicated by water contact angles. This study opens up new opportunities of exploring the heterogeneous characteristics of nanomaterials at environmentally relevant conditions.

## Conflicts of interest

There are no conflicts to declare.

## Acknowledgements

The authors gratefully acknowledge funding support from the NSF (Award ID : 1756444).

## References

1. M. Kalive, W. Zhang, Y. Chen and D. G. Capco, *Cell Biology and Toxicology*, 2012, **28**, 343-368.
2. K. Li, Y. Chen, W. Zhang, Z. Pu, L. Jiang and Y. Chen, *Chemical Research in Toxicology*, 2012, **25**, 1675-1681.
3. Y. Li, J. Niu, W. Zhang, L. Zhang and E. Shang, *Langmuir*, 2014, **30**, 2852-2862.
4. Y. Li, W. Zhang, J. Niu and Y. Chen, *ACS nano*, 2012, **6**, 5164-5173.
5. W. Zhang, Y. Li, J. Niu and Y. Chen, *Langmuir*, 2013, **29**, 4647-4651.
6. G. Sonavane, K. Tomoda, A. Sano, H. Ohshima, H. Terada and K. Makino, *Colloids and Surfaces B: Biointerfaces*, 2008, **65**, 1-10.
7. J. J. Faust, W. Zhang, B. A. Koeneman, Y. Chen and D. G. Capco, *Particle and fibre toxicology*, 2012, **9**, 42.
8. J. J. Faust, W. Zhang, Y. Chen and D. G. Capco, *Cell biology and toxicology*, 2014, **30**, 31-53.
9. R. D. Handy, R. Owen and E. Valsami-Jones, *Ecotoxicology*, 2008, **17**, 315-325.
10. C. Peng, W. Zhang, H. Gao, Y. Li, X. Tong, K. Li, X. Zhu, Y. Wang and Y. Chen, *Nanomaterials*, 2017, **7**, 21.
11. H. Y. Kim, J. O. Sofo, D. Velegol, M. W. Cole and A. A. Lucas, *Langmuir*, 2007, **23**, 1735-1740.
12. Y. Li, X. Chen and N. Gu, *The Journal of Physical Chemistry B*, 2008, **112**, 16647-16653.
13. R. Qiao, A. P. Roberts, A. S. Mount, S. J. Klaine and P. C. Ke, *Nano Letters*, 2007, **7**, 614-619.
14. K. Kostarelos, L. Lacerda, G. Pastorin, W. Wu, S. Wieckowski, J. Luangsivilay, S. Godefroy, D. Pantarotto, J. P. Briand, S. Muller, M. Prato and A. Bianco, *Nat. Nanotech.*, 2007, **2**, 108-113.
15. A. Verma, O. Uzun, Y. Hu, H. S. Han, N. Watson, S. Chen, D. J. Irvine and F. Stellacci, *Nat. Mater.*, 2008, **7**, 588-595.
16. X. Feng, L. Feng, M. Jin, J. Zhai, L. Jiang and D. Zhu, *Journal of the American Chemical Society*, 2004, **126**, 62-63.
17. H. S. Lim, D. Kwak, D. Y. Lee, S. G. Lee and K. Cho, *Journal of the American Chemical Society*, 2007, **129**, 4128-4129.
18. B. Yan, J. Tao, C. Pang, Z. Zheng, Z. Shen, C. H. A. Huan and T. Yu, *Langmuir*, 2008, **24**, 10569-10571.
19. C. Grabinski, N. Schaeublin, A. Wijaya, H. D'Couto, S. H. Baxamusa, K. Hamad-Schifferli and S. M. Hussain, *ACS Nano*, 2011, **5**, 2870-2879.
20. A. Albanese, P. S. Tang and W. C. W. Chan, *Annual Review of Biomedical Engineering*, 2012, **14**, 1-16.

21. W. Tungittiplakorn, C. Cohen and L. W. Lion, *Environ. Sci. Technol.*, 2004, **39**, 1354-1358.
22. H.-Q. Mao, K. Roy, V. L. Troung-Le, K. A. Janes, K. Y. Lin, Y. Wang, J. T. August and K. W. Leong, *J. Controlled Release*, 2001, **70**, 399-421.
23. P. Ghosh, G. Han, M. De, C. K. Kim and V. M. Rotello, *Advanced Drug Delivery Reviews*, 2008, **60**, 1307-1315.
24. M. Magomedov, *Phys. Solid State*, 2004, **46**, 954-968.
25. W. Zhang, A. G. Stack and Y. Chen, *Colloids and Surfaces B: Biointerfaces*, 2011, **82**, 316-324.
26. J. J. Kuna, K. Voitchovsky, C. Singh, H. Jiang, S. Mwenifumbo, P. K. Ghorai, M. M. Stevens, S. C. Glotzer and F. Stellacci, *Nature Materials*, 2009, **8**, 837-842.
27. P. Zhou, X. Zhu, J. Yu and W. Xiao, *ACS Applied Materials & Interfaces*, 2013, **5**, 8165-8172.
28. Y. Xiao and M. R. Wiesner, *Journal of Hazardous Materials*, 2012, **215-216**, 146-151.
29. M. S. Bell, A. Shahraz, K. A. Fichthorn and A. Borhan, *Langmuir*, 2015, **31**, 6752-6762.
30. A. Deak, E. Hild, A. L. Kovacs and Z. Horvolgyi, *Physical Chemistry Chemical Physics*, 2007, **9**, 6359-6370.
31. J. J. Kuna, K. Voitchovsky, C. Singh, H. Jiang, S. Mwenifumbo, P. K. Ghorai, M. M. Stevens, S. C. Glotzer and F. Stellacci, *Nat. Mater.*, 2009, **8**, 837-842.
32. H.-J. Butt, B. Cappella and M. Kappl, *Surf. Sci. Rep.*, 2005, **59**, 1-152.
33. T. Smith, *J. Colloid Interface Sci.*, 1980, **75**, 51-55.
34. G. R. Aiken, H. Hsu-Kim and J. N. Ryan, *Environ. Sci. Technol.*, 2011, **45**, 3196-3201.
35. M. Horie, K. Nishio, K. Fujita, S. Endoh, A. Miyauchi, Y. Saito, H. Iwahashi, K. Yamamoto, H. Murayama, H. Nakano, N. Nanashima, E. Niki and Y. Yoshida, *Chem. Res. Toxicol.* , 2009, **22**, 543-553.
36. K. M. Forward, A. L. Moster, D. K. Schwartz and D. J. Lacks, *Langmuir*, 2007, **23**, 5255-5258.
37. L. N. Arnaudov, O. J. Cayre, M. A. Cohen Stuart, S. D. Stoyanov and V. N. Paunov, *Physical Chemistry Chemical Physics*, 2010, **12**, 328-331.
38. O. J. Cayre and V. N. Paunov, *Langmuir*, 2004, **20**, 9594-9599.
39. B. M. Weon, J. San Lee, J. T. Kim, J. Pyo and J. H. Je, *Current opinion in colloid & interface science*, 2012, **17**, 388-395.
40. L. Isa, F. Lucas, R. Wepf and E. Reimhult, *Nature communications*, 2011, **2**, 438.
41. K. D. Hristovski, P. K. Westerhoff and J. D. Posner, *Journal of Environmental Science and Health, Part A*, 2011, **46**, 636-647.
42. P. Westerhoff and B. Nowack, *Accounts of chemical research*, 2012, **46**, 844-853.
43. W.-C. Hou, B. Y. Moghadam, P. Westerhoff and J. D. Posner, *Langmuir*, 2011, **27**, 11899-11905.
44. A. Praetorius, N. Tufenkji, K.-U. Goss, M. Scheringer, F. von der Kammer and M. Elimelech, *Environmental Science: Nano*, 2014, **1**, 317-323.
45. X. Xia, R. Baynes, N. Monteiro-Riviere and J. Riviere, *SAR and QSAR in Environmental Research*, 2007, **18**, 579-593.
46. X. Xia, N. A. Monteiro-Riviere and J. Riviere, *Nature nanotechnology*, 2010, **5**, 671.
47. Y. Xiao and M. R. Wiesner, *Environmental Science & Technology*, 2013, **47**, 2246-2253.
48. L. Thiele, H. P. Merkle and E. Walter, *Pharmaceutical Research*, 2003, **20**, 221-228.
49. X. Fang, B. Li, I. V. Chernyshova and P. Somasundaran, *The Journal of Physical Chemistry C*, 2010, **114**, 15473-15477.

50. S. Y. Cheng, R. Bryant, S. H. Doerr, C. J. Wright and P. R. Williams, *Environ. Sci. Tech.*, 2009, **43**, 6500-6506.
51. D. Alsteens, E. Dague, P. G. Rouxhet, A. R. Baulard and Y. F. Dufrêne, *Langmuir*, 2007, **23**, 11977-11979.
52. W. Fu, C. Carbrello, X. Wu and W. Zhang, *Nanoscale*, 2017, **9**, 15550-15557.
53. K. Voitchovsky, J. J. Kuna, S. A. Contera, E. Tosatti and F. Stellacci, *Nat. Nanotech.*, 2010, **5**, 401-405.
54. L. Sirghi, M. Nakamura, Y. Hatanaka and O. Takai, *Langmuir*, 2001, **17**, 8199-8203.
55. T. Eastman and D.-M. Zhu, *Langmuir*, 1996, **12**, 2859-2862.
56. O. Noel, M. Brogly, G. Castelein and J. Schultz, *Langmuir*, 2004, **20**, 2707-2712.
57. S. Deshpande, S. Patil, S. V. Kuchibhatla and S. Seal, *Applied Physics Letters*, 2005, **87**, 133113.
58. B. Wiley, Y. G. Sun, B. Mayers and Y. N. Xia, *Chem. Eur. J.*, 2005, **11**, 454-463.
59. C. C. Dupont-Gillain, B. Nysten, V. Hlady and P. G. Rouxhet, *J. Colloid Interface Sci.*, 1999, **220**, 163-169.
60. D. Marenduzzo, K. Finan and P. R. Cook, *J. Cell Biol.*, 2006, **175**, 681-686.
61. K. L. Chen and M. Elimelech, *Journal of Colloid and Interface Science*, 2007, **309**, 126-134.
62. W. A. Ducker and L. M. Grant, *J. Phys. Chem.*, 1996, **100**, 11507-11511.
63. S. C. Clear and P. F. Nealey, *J. Colloid Interface Sci.*, 1999, **213**, 238-250.
64. J. H. Park and N. Aluru, *Molecular Simulation*, 2009, **35**, 31-37.
65. A. Noy, S. Zepeda, C. A. Orme, Y. Yeh and J. J. De Yoreo, *Journal of the American Chemical Society*, 2003, **125**, 1356-1362.
66. C.-c. Chiu, P. B. Moore, W. Shinoda and S. O. Nielsen, *The Journal of chemical physics*, 2009, **131**, 244706.
67. N. Francesco De, C. Paola, S. Manuela, N. Francesca, C. Ilaria and C. Maurizio De, *Nanotechnology*, 2015, **26**, 145701.
68. J. I. Choi, S. D. Snow, J.-H. Kim and S. S. Jang, *Environmental Science & Technology*, 2015, **49**, 1529-1536.
69. K. L. Chen and M. Elimelech, *Langmuir*, 2006, **22**, 10994-11001.
70. F. A. I., R. A. G. and F. M. V., *ChemPhysChem*, 2010, **11**, 2612-2616.
71. N. Bizmark and M. A. Ioannidis, *Langmuir*, 2015, **31**, 9282-9289.
72. M. A. Chappell, A. J. George, K. M. Dontsova, B. E. Porter, C. L. Price, P. Zhou, E. Morikawa, A. J. Kennedy and J. A. Steevens, *Environmental Pollution*, 2009, **157**, 1081-1087.
73. H. Hyung, J. D. Fortner, J. B. Hughes and J.-H. Kim, *Environmental Science & Technology*, 2007, **41**, 179-184.
74. D. Zhang, B. Pan, R. L. Cook and B. Xing, *Environmental Pollution*, 2015, **196**, 292-299.
75. C. Zhang, L. Wu, D. Cai, C. Zhang, N. Wang, J. Zhang and Z. Wu, *ACS applied materials & interfaces*, 2013, **5**, 4783-4790.
76. Z. Yang, H. Yan, H. Yang, H. Li, A. Li and R. Cheng, *Water research*, 2013, **47**, 3037-3046.
77. X. Wang, L. Shu, Y. Wang, B. Xu, Y. Bai, S. Tao and B. Xing, *Environmental Science & Technology*, 2011, **45**, 9276-9283.